Asociación Argentina
de Mecánica Computacional

Mecánica Computacional Vol XXXIV, págs. 1989-2007 (artículo completo)
Sebastián Giusti, Martín Pucheta y Mario Storti (Eds.)
Córdoba, 8-11 Noviembre 2016

CAPABILITY OF THE PRESENT CAVITATING AND TURBULENCE MODELS FOR CONFINED FLOW SIMULATIONS

Miguel G. Coussirat[a], Flavio H. Moll[a] and Alfred Fontanals[b].

[a]*Grupo LAMA- Universidad Tecnológica Nacional-Facultad Regional Mendoza, Rodriguez 273 Ciudad 5500, Mendoza, Argentina; miguel.coussirat@frm.utn.edu.ar*

[b]*Departamento de Mecánica de Fluidos, EUETIB-Universitat Politècnica de Catalunya, España.*

Keywords: Cavitating Flow, Turbulence, Eddy Viscosity Models (EVM), Transport Equation-Based Model (TEM), Orifices, Validation/Calibration Tasks.

Abstract. Cavitating flow is a complex phenomenon closely related with turbulent and multiphase flows with mass transfer between the liquid and gaseous phases. This flow is affected by several factors as surrounding pressure, the local state of the turbulence, the non-condensable dissolved gases concentration and others. For studying this kind of flow several numerical models were developed and they are available in commercial and in-house software. A numerical model for cavitating flows involves a multiphase model, including a mass transfer submodel, and a turbulence model. Inside a commercial or an in-house numerical code there are several options and possible combinations of these models. To select the most suitable combination from this broad offer is not an easy task. This task involves also several decisions concerning a lot of calibration parameters that must to be defined in advance. The default values for these parameters are related to simple flow conditions, i.e., simple geometries and flows without any detachment. Under cavitation conditions these conditions are not the common situation. This work deals with the enhancement of some previous results obtained over simple geometries as orifices (injectors) with circular transversal sections. The model combinations that offered better results earlier are now studied more carefully. This study implies a detailed tuning of the production/dissipation coefficients of turbulence energy present in the turbulence models, and other parameters related to the cavitation state of the flow. It is known that these parameters have a strong influence over the numerical results obtained, both in terms of stability and accuracy. Also, a detailed comparison between mixture and volume of fluid models for modeling the multiphase flow was performed. The numerical results obtained were compared against experimental data for pressure, velocity and vapor fraction. In this work it is demonstrated that it is necessary to perform a careful calibration of both the turbulence and the cavitation models used, because there is a very close relation between the turbulence state of the flow, and the cavitation inception condition. A suitable calibration work allows us to diminish the mesh size (number of cells) saving a lot of computational resources too.

1 INTRODUCTION

Cavitation is a complex phenomenon that appears in a liquid flows when the hydrodynamic pressure falls out till values get nearer to the vapor pressure of the liquid, P_v. This low pressure provokes that the initial liquid flow becomes a two-phase flow (liquid-vapor bubbles), Brennen 1995. The initiation of cavitation by vaporization of the liquid may require that a negative stress exist because of surface stress tension and other effects. However, the presence of such things as undissolved gas particles, boundary layers, and turbulence will modify and often mask a departure of the critical pressure from vapor pressure, Knapp et al., 1970. The pressure drop is related both to the hydrodynamic flow and to the physical properties of the fluid, not only to the hydrodynamic flow. Under this pressure drop condition, the vapor bubbles appear and grow in size. When the pressure inside the bubbles exceeds the surrounding field pressure, the bubbles will suddenly collapse and condensate.

Steady and unsteady cavitating flows occur in many engineering systems from various applications, Coussirat et al., 2016. In most cases cavitation is an undesirable phenomenon (low performance and damage in materials) in other cases it is a useful application's tool. Some typical examples of low performance/damage in devices include cavitating flow into fuel injectors, liquid pumps, industrial turbomachinery, hydrofoils, marine propellers, hydrostatic bearings and bio heart valves, e.g. see Li et al., 2008. On the other hand, examples of utility of this phenomenon are water-jet cavitation peening (WCP) for improving fatigue strength and wear resistance of metals, e.g. see Zhang et al., 2013 or cavitating flow application used in a remarkable range of surgical and medical procedures, e.g. see Brennen 2006, and Brennen 2015.

In engineering applications, a designer must know details about cavitation inception, its location place, dynamics, structure, and relation to the damage produced on the solid walls that interact with the fluid in order to control cavitation behavior. In general the design process relies on a strong empiricism, because the theoretical developments available for study cavitating flows study are semi-empiric models. From a decade ago till now several numerical models have been developed and incorporated in commercial or in-house Computational Fluid Dynamics (CFD) codes. In spite of that, cavitating flows are still a big challenge for the numerical analysis using CFD codes, because cavitating flow modeling involves highly turbulent and two-phase flows. The availability of simple and reliable CFD codes for both turbulence and cavitation models that allow decreasing the computing power is still an open issue due to the fact that both turbulence and cavitation phenomena offer several challenges for a suitable modeling by means of the available CFD codes.

It is known that turbulence affects cavitation inception since a nucleus may be found in the core of a vortex where the local pressure level is lower than the mean value of the pressure in the flow. Hence, the nucleus could cavitate when it might not do so under the influence of the mean pressure level. This fact points out that cavitation may alter the global pressure field by altering the location of flow separation and the induced variations of the local turbulence level; thus, turbulence may promote cavitation and vice versa.

Although some details of these complicated viscous effects on cavitation inception were extensively examined by several authors in the past, (see Coussirat et al. 2016 for more

details), the effects such as the interaction of turbulence and cavitation inception have been recently identified more clearly. It is not surprising that any individual effect be readily isolated from many of the experiments performed in the past. To complete the list of those factors that may influence cavitation inception, it is necessary to remark the effects of surface roughness and the turbulence level in the flow too.

Concerning the applications of CFD codes for cavitating turbulent flows, it is normal to find both several EVM models for turbulence and continuum models for two-phase flows in a CFD code. However, the implementation of models for cavitating flow is more recent and not easily available. In the following paragraphs, some details concerning turbulence and cavitation models will be given, for more details see Coussirat et al., 2016.

1.1. Turbulence Modeling

Nowadays, the common option for industrial turbulent flows is the Reynolds-averaged Navier–Stokes (RANS) equations (or Reynolds-Averaged Simulations, RAS), plus an Eddy Viscosity Model (EVM) for closing the equations system. For CFD applied to industrial flows, EVMs called One- and Two- equations EVM are the most popular in the CFD community. The aforementioned names are related to the number of differential equations used for computing the turbulence level (momentum exchange among fluctuating velocities). These partial differential equations (PDEs) are transport equations for representative turbulence quantities (i.e., representative scales of turbulence, e.g., see details in Tennekes et al., 1973, Wilcox, 1994 and Durbin et al., 2001). These PDEs include: local acceleration, convection, production, turbulent transport and diffusion of these quantities. By solving these equations, finally an eddy viscosity, ν_t, is computed, incresing in this way the dissipative effect of the molecular viscosity.

Models available in commercial CFD software comprise the One- equation model from Spalart and Allmaras (so called SA), and several models of Two- equations. Popular Two-equation models are: the Standard k-ε, the RNG k-ε, the Realizable k-ε, the Standard k-ω and the Shear Stress Transport k-ω (SST k-ω). Details of this kind of models are given in Spalart et al., 1994, Wilcox, 1994, Menter, 1994, Durbin et al., 2001, Menter et al., 2003, Coussirat 2003 and Versteeg et al., 2007. More sophisticated options such as Reynolds Stress Models (RSM), Large-Eddy Simulation (LES), or some kind of hybrid models that use a "mixture" of LES and EVM options are also available (e.g. see Coussirat 2003, Versteeg et al., and 2007Menter et al., 2010). LES and hybrid models are more difficult to use in industrial CFD due to the fact that these models are more expensive in terms of the necessary computational resources, (e.g., see Coussirat 2003, Sagaut, 2006, Chunekar, 2009, Goncalves et al., 2009, Salvador et al., 2013, Sou et al., 2014).

Some examples in order to estimate the CPU cost for LES computational requirement for cavitating flow in Venturis are given in Spalart, 2000 and Coussirat et al., 2016. Then, the computing resources required for such a large grid make the LES simulations practically unfeasible for industrial flow simulations. Hence, the optimization of EVM turbulence models for expanded categories of flows is still a useful and necessary option nowadays. At the moment, a great amount of the CFD research related to the turbulence consists of case-by-case examination and validation/calibration tasks of existing turbulence models for such specific problems.

1.2. Cavitating Flow Modeling

Concerning the specific strategies available for modeling cavitating flows, several numerical models were developed and they can be classified into two main categories: fitting interface and continuum modeling (i.e., homogeneous flow theory, see Senocak, 2002 and Chunekar, 2009 for details). Fitting methods are generally used for simulating steady sheet cavitation, Brennen, 1995. The cavitation region is assumed to be at a constant pressure equal to the vapor pressure of the liquid and bounded by a distinct liquid–vapor interface.

The interface is tracked based on the constant pressure assumption, while the closure region of the cavity is approximated by a wake model. Limitations of this kind of model are the impossibility of transient cavitation modeling and the incomplete recovering of the detailed physics of cavitation.

The second category of models, i.e., homogeneous models or continuum modeling, is becoming popular because it includes the physics of cavitating flows and can be easily implemented. More in detail, in homogeneous models the mixture density concept is introduced and a single set of mass and momentum equations are solved. Differences between the various models in this category mostly come from the relation that defines the variable density field. Some of the existing studies solve the energy equation and determine the density by means of suitable equations of state. Since most cavitating flows are isothermal, arbitrary barotropic equations have been proposed to supplement the energy consideration, Senocak et al., 2002. Another popular approach is the transport equation-based model (TEM), where a transport equation for either mass and volume fraction, with appropriate source terms for regulate the transfer between phases, is solved. A quite complete description of all of these models can be seen in Senocak, 2002.

The implementation of these models is performed using different approaches: single fluid, two-fluid models, and hybrid models. Hybrid models are between the one fluid and two fluids (or three fluids) ones; they are based on an equation of mass transport, adding source terms related to the effects of cavitation (bubble generation and its collapsing, see details in Kunz et al., 1999, Singhal et al., 2002, Goncalves et. al., 2009, Chunekar, 2009, and Rodio et al., 2015). The derivation of these source terms related to cavitation effects affecting the mass equation is made from different assumptions and simplifications of the Rayleigh–Plesset equation (see details in Kubota et al., 1992, Singhal et al., 2002, Zwart et al., 2004 and Franc and Michel 2004). One of the most recent and widespread models is referred to as the "complete model" or "full cavitation model" from Singhal et al., 2002. This one is based on the use of RANS equations plus a "closing model" (EVM or other) for turbulent flow and for fluids with variable density. This density variation is a function of the vapor fraction which in turn is computed by solving a mass transport equation for it, taking into account all first-order effects, such as phase change, bubble dynamics, turbulent pressure fluctuations, and non-condensable gases. Another model of common use is the Zwart et al., 2004 (also called ZGB model), being a simplification of the Singhal model; assuming that all the bubbles in a system have the same size and the total interphase mass transfer rate per unit volume can be calculated using the bubble density numbers with the mass change rate of a single bubble.

The adequacy of TEM models compared to ones that use a barotropic equation of state is supported by experimental evidence from Gopalan et al., 2000 showing that vorticity production

occurs at the closure region of sheet cavities due to baroclinic torque, therefore if an arbitrary barotropic equation is used, the gradients of density and pressure are always parallel; hence the baroclinic torque is zero. This fact suggests that physical models that utilize a barotropic equation will fail to capture an experimentally observed characteristic of cavitating flows. Likewise, solving an energy equation will also experience the same situation if the flow is essentially isothermal. On the other hand, in TEM approach the density is a function of the transport process. Consequently, gradients of density and pressure are not necessarily parallel, suggesting that TEM can accommodate the baroclinic vorticity generation.

At the moment of applying these models for solving industrial problems, the designer must know in advance which a suitable setup could be for each of these models. The use of turbulence and cavitation models implies the management of several parameters, in order to obtain a good calibration of these models. The definition and fitting of these parameters relies in the own knowledge of the developers of these models. The information about how to use these calibration parameters available in the CFD codes documentation is not clear for the user of these models, (see e.g. Ansys 2015).

It was highlighted that the turbulence level in the flow is one of the most important parameters that define the cavitation inception. Therefore, a suitable turbulence modeling is necessary for obtaining good results by means of CFD to compute cavitating flows. Thus, the main goal of this work is aimed at gaining a deeper knowledge in the calibration of some turbulence models already assessed in previous works (see complete details in Moll et al., 2011, Moll et al., 2012, Gandolfo et al., 2013, Cappa et al., 2014 and Coussirat et al., 2016). All of the aforementioned works are related to obtaining suitable options for EVMs by means of careful studies of their behavior. It is interesting to highlight that in the work from Coussirat et al., 2016 it was demonstrated that a suitable calibration of the turbulence model used is more important than a fine tuning of the cavitation model.

2 APPLIED METHODOLOGY

First, a more extensive survey and analysis of CFD works related with cavitating flows in orifices and nozzles was made. For fuel injectors (orifices), several CFD simulations using the Standard k-ε, the Realizable k-ε and the Standard k-ω models coupled with a TEM model (i.e., Singhal or ZGB model) for modeling turbulence and cavitation respectively were found in the literature. There are only few works relating the SA model with cavitation models (e.g., Moll et al., 2011, Moll et al., 2012). Unfortunately, only the orifice's discharge coefficient, C_d, was used for validation/calibration tasks in the majority of CFD results related to cavitating flow in orifices found in the literature. This is a mean parameter that does not precisely represents the behavior of the cavity, because it only accounts for the mass flow variations, without any description of the details related to the pressure variations along the wall, local velocity profiles or local vapor fraction profiles. At present, it is even more difficult to find works using some of these 'local' variables or profiles for models validation/calibration, because they are scarce, see more details in Sou et al., 2014 and Coussirat et al., 2016.

For convergent-divergent nozzles some information related with steady and unsteady cavitation can be seen in Stutz et al., 1997a, Stutz et al., 1997b, and Stutz et al., 2000. Details related to experiments and CFD simulations using several EVMs can be seen in Barre et al., 2009, Goncalves et al., 2009, and Gandolfo et al., 2013. Numerical simulations using several EVMs coupled with the Singhal and ZGB cavitations models where presented by Moll et al.,

2011, Moll et al., 2012, Gandolfo et al., 2013. A comparison of the CFD results obtained against experimental ones, both for velocity and vapor fraction profiles in several places along the Venturi geometry was performed. The main conclusion of this analysis is that no clear superiority of one turbulence model over other was observed. Lu et al., 2009, presents CFD results using several Two-equation EVMs for turbulence, investigating the applicability of the Standard k-ε, the RNG k-ε and the Standard k-ω turbulent models for cavitation in a water jet field through a convergent-divergent nozzle. The result showed by the Lu's study indicated that the RNG k-ε turbulence model is the most suitable for the simulation of cavitation behavior for this case, but no comments related to the EVM calibrations parameters were presented. Therefore, the idea of a possible performance improvement of these EVMs by means of modifications of their calibrations parameters is an interesting option that has not been fully explored yet, despite some work exploring this option has been carried out (e.g. see Bardow et al., 2008, Cappa et al., 2014 and Coussirat et al., 2016).

2.1 EVMs Turbulence Model Parameters Calibration

In general, the transport equations in an EVM have several terms (production, turbulent transport, dissipation, etc.). The majority of these terms have many calibration coefficients, normally tuned for simple attached flows (e.g., boundary layers without or with slight adverse pressure gradients both in confined or not confined single- phase flows), and for simple geometries (e.g., flat plates, smooth blade profiles, pipes, etc.). Particularly, the impact of these model parameters in different classes of application scenarios is not fully understood (Coussirat 2003). A systematic approach for assessing their impact involves optimization methods for CFD that allow quantitative model analyses by a rigorous comparison against experimental data. In relation to the turbulence parameter calibrations, the viewpoints stated in Bardow et al., 2008, help to gain insight in this subject. Unfortunately, this study involved a non-cavitating flow between plane plates and not so for orifices with cavitating flow. An extension of this kind of analysis to cases of cavitating flows in orifices was made by Cappa et al., 2014 and Coussirat et al., 2016. These works were carried out bearing in mind the CFD results obtained by Coutier-Delgosha et al., 2003, showing that the CFD results can be improved by increasing the turbulent viscosity, ν_t, in some way in the formulation of the Standard k-ε turbulence model. Also, the work from Spalart and Allmaras et al., 1994 points out that in anisotropic flows, the ν_t can increase only by modifying the effects of its production.

Following these ideas, and after a careful study of the structure of the selected EVMs (two models, i.e., the SA, and the SST k–ω models), a detailed calibration of the coefficients related to the turbulence (coefficients affecting the ν_t value, or coefficients affecting production/dissipation terms) was made. At present, the SA model, a One-equation turbulence model, has several versions. The original version is presented here (Eqs.1-3). In this model ν_t is directly determined by a transport equation (see full details in Spalart and Allmaras et al., 1994).

$$\nu_t = \tilde{\nu} f_{v1} = \tilde{\nu}\left[\frac{(\tilde{\nu}/\nu)^3}{(\tilde{\nu}/\nu)^3 + {c_{v1}}^3}\right] \tag{1}$$

$$\rho\frac{D\tilde{\nu}}{Dt} = \rho c_{b1}\tilde{S}\tilde{\nu} + \frac{1}{\sigma_{\tilde{\nu}}}\left[\frac{\partial}{\partial x_j}\left\{(\mu+\rho\tilde{\nu})\frac{\partial\tilde{\nu}}{\partial x_j}\right\} + \rho c_{b2}\left(\frac{\partial\tilde{\nu}}{\partial x_j}\right)^2\right] - \rho c_{w1} f_w \frac{\tilde{\nu}}{d^2} \tag{2}$$

$$C_{w1} = f(C_{v1}, \kappa, C_{b2}, \sigma_{\tilde{\nu}});\ f_w = f(C_{w2}, C_{w3}) \tag{3}$$

Instead, in the SST ***k–ω*** model, a Two-equation turbulence model, the turbulent (eddy) viscosity, ν_t, is computed by means a combination of two variables representing velocity and length scales of turbulence (i.e., the turbulent kinetic energy, ***k*** and its rate of dissipation, ***ω***). Values for these two turbulence scales are computed by transport equations of each scale, Eqs.4-7):

$$\nu_t = \alpha^* \rho k \omega^{-1}, \omega = \varepsilon k^{-1};\ S_{ij} = \frac{1}{2}\left(\frac{\partial u_j}{\partial x_i} + \frac{\partial u_i}{\partial x_j}\right); \tag{4}$$

$$\frac{\partial k}{\partial t} + u_i \frac{\partial k}{\partial x_i} = 2\nu_T S_{ij} S_{ji} + \frac{\partial}{\partial x_i}\left[\left(\frac{\nu_T}{\sigma_k} + \nu\right)\frac{\partial k}{\partial x_i}\right] - \beta^* f_{\beta^*} k\omega \tag{5}$$

$$\frac{\partial \omega}{\partial t} + u_i \frac{\partial \omega}{\partial x_i} = \alpha\left(\frac{\omega}{k}\right) 2\nu_T S_{ij} S_{ji} + \frac{\partial}{\partial x_i}\left[\left(\frac{\nu_T}{\sigma_\omega} + \nu\right)\frac{\partial \omega}{\partial x_i}\right] - \beta\, f_\beta\, \omega^2 \tag{6}$$

$$\mathrm{Re}_t = \rho k(\mu\omega)^{-1};\ \alpha^* = f(\alpha, \beta_i, \mathrm{Re}_t, R_k) \tag{7}$$

Where $\sigma_k, \sigma_\omega, \alpha, \beta, \beta^*, \beta_i, \beta_\infty^*, \mathrm{Re}_t, f_\beta, f_{\beta^*}$ are empirical functions, and constant values (see full details in Menter, 1994 and Menter et al., 2003). The set of equations Eqs.1-7, is a summary of the models used (SA and SST ***k–ω***), and here, only a brief explanation of them is given, not showing the complete set of parameters that the models have. They look very complex for the user that does not know full details of these models, due to the fact that there are a lot of parameters for performing calibration tasks.

In this work, an analysis for identifying which of these parameters affecting more the computed levelof ν_t was carried out, taking into account that it is necessary to have low levels of ν_t for a suitable prediction of the cavitation inception, following the ideas of Spalart et al., 1994, Bardow et al., 2008 and Coutier-Delgosha et al., 2003. This preliminary analysis was necessary for carrying out the subsequent sensitivity parameter analysis that will be performed.

In the SA model, equation, Eq.2 takes into account the production, transport and dissipation of ν_t. Then for having lower levels of ν_t, it is necessary to have lower levels of ν_t by itself or for its production. Another possibility is to have higher levels of the dissipation of ν_t. In all cases these effects are obtained by means of changes in the associated calibration coefficients. On the other hand, in the SST ***k–ω*** model from Menter, 1994, the equations Eq.5-6 are the transport equations for turbulence scales (***k*** and ***ω***) used for computing the levels of ν_t. Similarly to the SA model, the equations take into account the production, transport and dissipation of these scales, but ν_t is computed after solving these PDEs, by means of a suitable combination of them, see Eq.4.

After this preliminary analysis, a subsequent sensitivity analysis (not shown here) was carried out. This one has consisted of using a base case for CFD computations of cavitating flows by using both the SA and the SST ***k–ω*** models with the default setting of all parameters to study (see details in Section 3). Values and parameters representative of turbulence (e.g., ν_t by itself, the turbulent/molecular viscosity ratio, $\tilde{\nu}/\nu$, the turbulent kinetic energy, ***k***, its dissipation, ***ω*** and others) in zones where the cavitation inception appears, were computed.

Afterwards, a study of sensitivity for several fitting parameters related with the turbulence level was performed using these computed values as 'input data'. The study was performed both for the SA and the SST k–ω models. These 'input data' allow to calculate 'by hand' some trends in the results of ν_t when the selected parameters are modified.

It was observed that in general, there is a "monotonic" influence over the terms that certain parameter affects, in the sense that the variations follow potential laws, without local maxima or minima values.

In this way, the most relevant parameters were selected for the sensitivity study, by running several cases using the setup described in Section 3. For the SA model the parameters selected for calibration were: C_{v1}, a 'global parameter' related directly to ν_t (Eq.1) and C_{b1}, a 'local parameter' related to the value computed for the production of ν_t (first term on the right in the Eq.2). Instead, for the SST k–ω model, the parameters selected for calibration were: β_i, a 'global parameter' closely related to α^*, that affects the computation of ν_t (Eq.4) and β_∞^*, a 'local parameter', correlated to the value of β^*, responsible of the computed level of the dissipation of turbulent kinetic energy, k (last term on the right in the Eq.5).

3 CFD MODEL DEFINED AND DISCUSSION OF THE RESULTS OBTAINED

A commercial code (ANSYS/FLUENT v12) was used to model a turbulent cavitating flow in an orifice injector. The simulated geometry was an axi-symmetrical 2D model of a round nozzle (Fig.1). The database from Nurick, 1976 was selected, because it is well documented and broadly used by the CFD community for cases of cavitating flows in injectors. This set of data is related to orifices/nozzles of several geometries. One of the well documented case within this database is a round nozzle of Lucite material with the following characteristics: a outlet diameter, d=7.62mm, a ratio of inlet/outlet orifice diameters, D/d, equal to 2.88, and a ratio of orifice length/outlet orifice diameter, L/d, equal to 5.0.

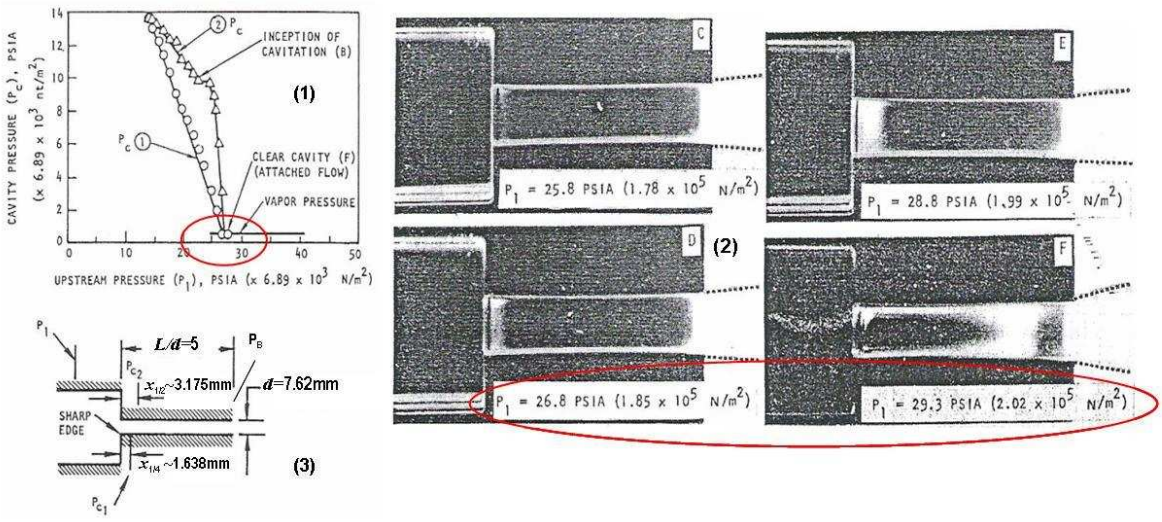

Fig. 1: Experiment from Nurick, 1976. (1) Cavity pressures P_{C1} and P_{C2}. (2) Cavity shape evolution when inlet pressure P_1 was changed. The plateau in the curve (25.8 PSIA (1.773×10^5 Pa) $<P_1<$ 28.5 PSIA (1.963×10^5 Pa), encircled in red) is correlated with the fuzzy region that appears near the inlet in the pictures (this is a not clear fact for the authors, see details in Peterson, 1977). (3) Nozzle geometry: P_{C1} and P_{C2} are static taps pressure, placed at ~0.25d and ~0.5d respectively downstream of the orifice (see more details in Coussirat et al., 2016).

The available data are: 1. Static pressure measurements $\boldsymbol{P_{c1}}$ and $\boldsymbol{P_{c2}}$ at two positions along the length $\boldsymbol{L}$ i.e., distances $\boldsymbol{x_{1/4}} \sim \boldsymbol{d}/4$ and $\boldsymbol{x_{1/2}} \sim \boldsymbol{d}/2$ respectively from the contraction, see Fig.1(1). 2. Some pictures showing the structure of the cavity, see Fig.1(2). 3. For other $\boldsymbol{D/d}$ ratio ($\boldsymbol{D/d}$ =12) there are mass flow measurements expressed by means of a discharge coefficient $\boldsymbol{C_d} = f(\dot{m}, A_B)$, see Eq.8, for ratios $\boldsymbol{L/d}$=6.0, 10 and 20 (not shown here). Based on its experimental results Nurick, 1976 proposed a theoretical correlation, Eq. 8, for computing the coefficient $\boldsymbol{C_d} = f(\sigma)$ under cavitation conditions for all cases, taking this correlation as an experimental approach to compute $\boldsymbol{C_d}$ for comparison against numerical results obtained.

$$C_d = \frac{\dot{m}}{A_B\sqrt{2\rho_l\left(P_1 - P_B\right)}} = \underbrace{C_c\sqrt{\sigma}}_{\text{Nurick correl.}};\ \sigma = \frac{P_1 - P_v}{P_1 - P_B}, C_c = \left[0{,}62 + 0{,}38\left(\frac{d}{D}\right)^3\right] \tag{8}$$

Where: $\boldsymbol{A_B}$, is the outlet section of the orifice; $\dot{m}$, is the mass flow rate; ρ_l, is the liquid phase density; $\boldsymbol{P_1}$ and $\boldsymbol{P_B}$, are the nozzle inlet and outlet pressure imposed; $\boldsymbol{P_v}$, is a certain critical pressure. This critical pressure value is taken equal to the vapor pressure, despite that undissolved gas particles, boundary layers, and turbulence level could modify and often mask a departure of the critical pressure from vapor pressure. As a consequence, a non-dimensional coefficient, $\boldsymbol{\sigma}$, as been adopted as the parameter for comparison of vaporous cavitation events, Knapp et al., 1970.

3.1. Defining the CFD Setup

The geometry selected for modelling was the Nurick case, $\boldsymbol{D/d}$=2.88, $\boldsymbol{L/d}$=5, and Lucite material (see full details in Nurick, 1976). Flow separation and reattachment CFD estimations are strongly dependent on a correct prediction for the development of the near-wall turbulence and its instability. Nurick points out that a very stable cavity was observed in this case; therefore, a steady flow was simulated in this work. This decision was reinforced by means of computing the Strouhal number, **Sr,** being $\mathbf{Sr}=\boldsymbol{d}\times(\boldsymbol{t}\times\boldsymbol{c_B})^{-1}$, where: $\boldsymbol{d}$ is the orifice diameter, $\boldsymbol{t}$ is the characteristic time of the unsteadiness and $\boldsymbol{c_B}$ is the mean flow velocity at the outlet. A value of Sr~O(10^{-2}) was computed, showing that this case, ($\boldsymbol{D/d}$=2.88, $\boldsymbol{L/d}$=5 geometry), looks like a steady phenomenon correlated with low frequencies (see more details in Coussirat et al., 2016).

Experiments also show that for the setups of the case where $\boldsymbol{P_1}>2.0\times10^5$Pa ($\boldsymbol{D/d}$=2.88 and $\boldsymbol{L/d}$=5 geometry), the cavitation becomes developed and almost at the same time the flipping (i.e., a detachment of the flow from the orifice wall without cavitation in a jet fashion) appears, suppressing the previously developed cavitation state (see more details in Nurick, 1976 and Coussirat et al., 2106). This flipping condition is a severe restriction for CFD simulations, because the flow changes from cavitating flow to a free jet one, a completely different kind of fluid flow. Therefore, a careful approximation to this condition is necessary in order to avoid the instability related to the change of the flow type. This fact is not taken into account by several authors found in the literature (see more details in Coussirat et al., 2016).

Thus, the cavitation inception condition was defined in the same way as experiments, i.e., onset of cavitation is within the range of $1.85\times10^5\text{Pa}<\boldsymbol{P_1}<2.0\times10^5$ Pa, see Fig.1, despite that lower or upper boundary $\boldsymbol{P_1}$ values were set in some cases, see Table 1. Therefore, pressure boundary conditions were defined both for the inlet and outlet boundaries, by means of a $\boldsymbol{P_1}$ variable inlet and a constant value for the outlet, $\boldsymbol{P_B}$=95,000Pa.

Table 1: Case (***D/d***=2.88, ***L/d***=5): CFD cases modeled. (SA and SST ***k–ω*** models combined with the Singhal model). Each case was defined by setting an inlet pressure value, P_1 selected from Nurick data, see Fig.1(1). P_B=95,000Pa in all cases. The equivalent cavitation number (σ) for each value of P_1 was computed using Eq.8.

P_1	1.50e5	1.64e5	1.85e5	2.02e5	2.20e5	2.30e5	2.40e5	2.50e5
σ	2.67	2.33	2.00	1.85	1.73	1.68	1.63	1.59

For defining the mesh size, the sensitivity mesh analysis (comparison of CFD results between several meshes, and 2D and 3D cases), already performed in Coussirat et al., 2016 was used as reference. This allows the use of a quadrilateral structured mesh of 12,800 cells. The range obtained for y^+ with this mesh was $15<y^+<65$. It is necessary to take into account that the grid convergence studies with wall functions approach fail in some cases because the wall boundary condition is ill-posed. Here, the inner limit was defined for the standard wall functions at a value of y^+~11(laminar sublayer) for a well-posed 'wall function' boundary condition (see details in Ansys 2015), although the selected turbulence models do not use this wall treatment. This is a useful observation pointed out to save CPU resources for future applications in modeling complex 3D flow cases with turbulence models that need a near-wall boundary condition. On the other hand, notice that to take into account the needed computational resources in 3D cases, a simple 180^o evolving from the 2D geometry around the symmetry axis generates a 3D mesh of around 3.0×10^6 cells for the already defined mesh (see details in Coussirat et al., 2016).

In commercial CFD codes, there are several possibilities for combining turbulence and cavitation models taking into account that two-phase flows can be modelled by means of the Mixture model or the Volume of Fluid (VOF) model (see details in Ansys 2015). By using the combinations of several turbulence models together with the cavitation models, Coussirat et al., 2016 showed that the SA and SST ***k–ω*** turbulence models together with the Singhal cavitation model proved to be the best combination of EVMs/cavitation models for nozzles. But, in this previous work, only the mixture model was used.

Finally, the following setup for a CFD modelling of the ***D/d***=2.88, ***L/d***=5 geometry case, from Nurick was defined, including: 1) The combination of the SA and SST ***k–ω*** turbulence models together with the Singhal cavitation model. 2) Second-order upwind schemes for all the equations (flow and turbulence), except for the vapor transport equation, where the 'QUICK' scheme was selected. 3) For the pressure–velocity coupling, the 'SIMPLE' scheme was selected. 4) The dissolved gases contained into the liquid phase were defined in a value of 10^{-9} ppm. 5) Normalized residuals of $O(10^{-5})$ were imposed, and computations were made in double precision. It is highlighted that, with this setup, also a complementary analysis of the performance of the Mixture and VOF models was performed to check the differences between them, using both Singhal and ZGB models for cavitation modeling. Results obtained showed that there were negligible differences in all the cases modelled (not shown).

3.2. Results Obtained for the Discharge Coefficient C_d

The CFD results obtained for the C_d using this setup and for changes in the parameters related to the turbulence modeling are shown in Fig.2, and Fig.3. Experimental values from Nurick for $\dot{m}$, P_{c1} and P_{c2}, for several values of the inlet pressure imposed, P_1 (nearer to the cavitation inception) are given in Table 2 for comparisons.

Fig.2 shows that the SA/Singhal combination predicted lower values for C_d for of cavitation number, σ<1.75 and higher C_d values within the range of 1.60<σ<1.75, (i.e.,~2.50×10^{5}Pa>P_1>~2.20×10^{5}Pa). The flipping phenomenon showed by the experiments, i.e., a sudden falling in C_d values for σ~1.75 is not captured by these combinations of models.

Table 2: Case (D/d=2.88, L/d=5): Experimental values for $\dot{m}$, and P_{c1} and P_{c2} pressure values, 1.64×10^5<P_1 <2.02×10^5 from Nurick database.

P_1 [×10^5 Pa]	σ	$\dot{m}$ [kg/s]	P_{c1} [Pa]	P_{c2} [Pa]
1.64	2.33	0.51	~32,200	~66,000
1.85	2.02	0.54	3,540	~21,100
2.02	1.85	0.56	3,540	3,540

On the other hand, the combination of SST k–ω -/Singhal models shows some trend to capture the flipping phenomenon, but not for the default value of β_∞*, see Fig.3. Only the extreme values for this coefficient show a better agreement with the experimental C_d values (see red symbols in Fig. 3).

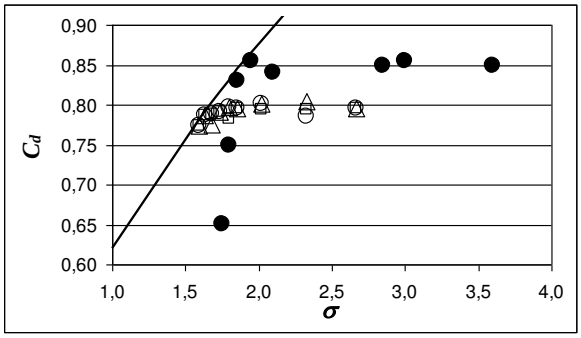

Fig. 2: CFD, SA/Singhal models: C_d vs. σ.
Notation: –Theor.Nurick, correl.; ♦ Exp.Nurick
L/d=6, D/d=12, Symbols C_{v1} values:
□ =4.0;**O**=7.1;Δ=10.0.

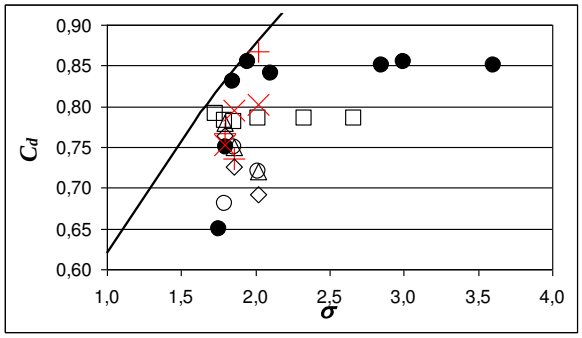

Fig. 3: CFD, SST k–ω/Singhal models: C_d vs. σ.
Notation: – Theor. Nurick, correl.; ♦ Exp. Nurick
L/d=6, D/d=12; Symbols β_∞* values:
+ =0.20; **O**=0.18; Δ=0.15; □=0.09; ◊=0.09;×=0.05

This is an interesting result, owing to the fact that the previous sensitivity analysis showed a monotonic influence of this parameter on the dissipation term in the k equation, Eq.5. A reason for this fact could be that it is not an easy task to analyse the complete influence of this parameter in the model equations. More research will be necessary for having a clearer knowledge of this behaviour.

It is pointed out that the work of Coussirat et al., 2016 showed that using a similar mesh (12,800 cells) as the mesh used in the present work, the flipping phenomenon is not captured by setting the default values for the coefficients, i.e. C_{v1}, C_{b1}, for the SA model; and β_∞*, $\beta_{1,ineer}$, for the SST k–ω model respectively. For capturing the flipping without any calibration, bigger meshes were required (~75,000 cells). Thus, the present sensitivity analysis shows that it is possible to improve results for cavitating flows in conditions nearer the flipping flow by using lower size meshes combined with well calibrated turbulence models.

3.3 Results Obtained for the Wall Pressures P_{C1} and P_{C2}

Concerning the wall pressure fittings obtained, (i.e., P_{C1} and P_{C2}), the results obtained are shown in Fig 4 and Fig 5 for the SA/Singhal combination and Fig 6 and Fig 7 for the SST k–ω/Singhal combination respectively. For reference, in Table 3 the numerical results obtained with the SA by Coussirat et al., 2016, are shown. Better fittings for P_{c2} pressures values, but not for P_{c1} ones were obtained when the coefficient C_{b1} decreases. Notice that there is no a big variation in the mass flow coefficient C_d predicted for all values of C_{b1}, showing that there is not a high correlation between C_d (correlated to the mass flow) and the local pressure variations near the orifice.

Fig.4, Fig. 5, and Table 4 show the numerical results obtained in the present work (SA/Singhal models), now for variations of C_{v1} but maintaining the default value for the C_{b1} coefficient (i.e., C_{b1} =0.1355).

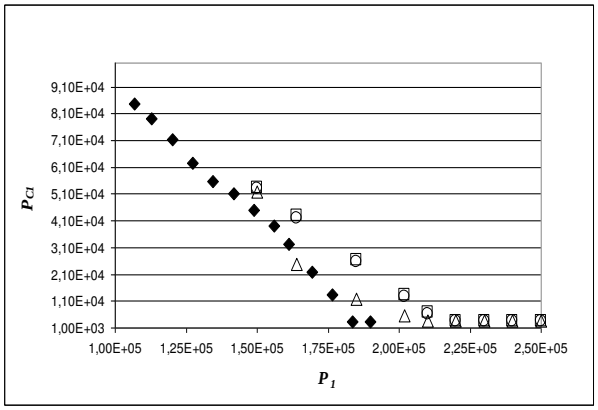

Fig. 4: CFD, SA/Singhal models: P_{c1} vs. P_1.
Notation: ♦ Exp.Nurick L/d=5.0, D/d=2.88,
Symbols C_{v1} values: □ =4.0; o=7.1; Δ=10.0.

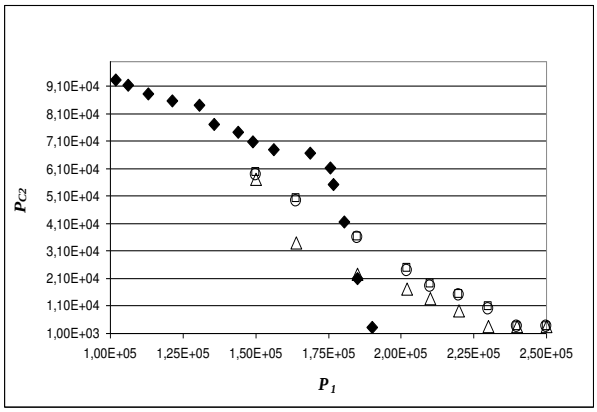

Fig. 5: CFD, SA/Singhal models: P_{c2} vs. P_1.
Notation: ♦ Exp.Nurick L/d=5.0, D/d=2.88,
Symbols C_{v1} values: □ =4.0; o=7.1; Δ=10.0.

Results obtained show that when lower values for C_{v1} were imposed, the wall pressure values were better fitted. Notice that both for C_{b1} and C_{v1} coefficients, the variations are monotonic as could be expected due to the behaviour of them when the sensitivity analysis was performed. This sensitivity study shows better predictions of the wall pressures P_{c1} and P_{c2} when the coefficient values selected allow to decrease the ν_t level, being the discharge coefficient C_d less sensitive to these changes.

Table 3: CFD results from Coussirat et al., 2016: **SA** model, 12,800 cells mesh and P_1=2.02e5 Pa. Values obtained for: the mass flow [kg/s], P_{c1} and P_{c2} pressures [Pa], by changing the values of the C_{b1} coefficient in the production term, (turbulent viscosity equation, ν_t. The box into the Table points out the values used for C_{b1}.

Reference parameter	Nurick Exp.	**CFD results.** Columns in **bold**: Results obtained for the reference (default) value of C_{b1} =**0.1355**					
		Set of values for C_{b1}					
		0.0700	0.0850	0.1000	**0.1355**	0.1500	0.1700
Mass flow [kg/s]	0.562	0.528	0.526	0.527	**0.528**	0.529	0.529
Pressure, P_{c1} [Pa]	3,540.000	11,282.30	12,287,39	11.696,68	**11,127.17**	10,990.60	10,965,56
Pressure, P_{c2} [Pa]	3,540.000	14,011.48	16,700.25	17,803,69	**21,973.74**	24,086.19	27,445.21

Despite the better fitting of the P_{c1} and P_{c2} obtained, the cavitation inception is not captured because the pressure values predicted are still high. Combination of higher values for C_{v1} with lower values for C_{b1} should give better pressure fittings. Notice that C_d predictions were insensitive to changes both in the C_{v1} (Table 3) and the C_{b1} (Table 4) coefficients. The reason of this behavior could be attributed to the fact the C_d is a 'global parameter' accounting for a mean value of the mass flow.

Results obtained with the SST k–ω /Singhal models combination, are shown in Fig.6, Fig.7, Table 5 and Table 6. Only high values of β^*_∞ give better fittings of the pressure P_{c1} and P_{c2}, although C_d was also well predicted setting low values for β^*_∞. Both P_{c1} and P_{c2}, reach the vapour pressure value but with some convergence problems. This could be due to the fact that under this condition the cavitating flow becomes a flipping jet flow and a cavitation model starts to be inadequate for the flow modeling because a flipping jet flow needs an unsteady Volume Of Fluid (VOF) modeling technique.

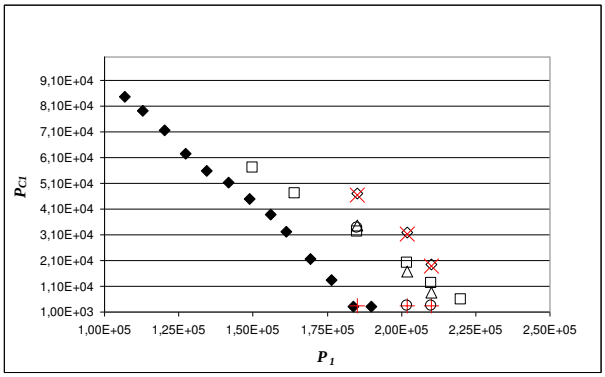

Fig. 6: CFD, SST k–ω models: P_{c1} vs. P_1.
Notation: ♦ Exp. Nurick L/d=5.0, D/d=2.88;
symbols β_∞* values: + =0.20; o=0.18; Δ=0.15;
□=0.09; ◊=0.09;×=0.05.

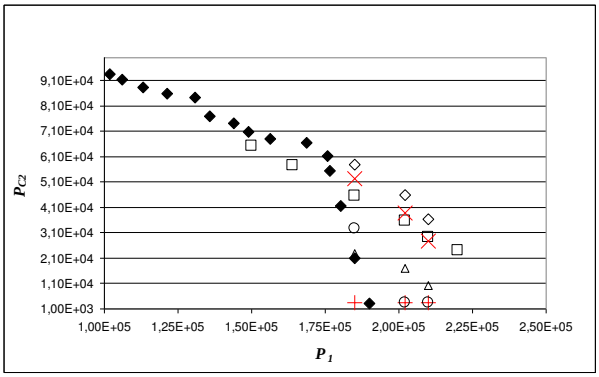

Fig. 7: CFD, SST k–ω - Singhal models: P_{c2} vs. P_1.
Notation: ♦ Exp. Nurick L/d=5.0, D/d=2.88;
Symbols β_∞* values: + =0.20; o=0.18; Δ=0.15;
□=0.09; ◊=0.09;×=0.05

On the other hand, changes in the $\beta_{1,inner}$ coefficient do not show big sensitivity in the pressure fitting, and the trend in predictions is not monotonic. Minimum pressure values for P_{c1} and P_{c2} were reached when $\beta_{1,inner}$=0.095 (see Table 5).

Table 4: CFD results for the SA/Singhal models, mesh of 12,800 cells and variable values of P_1. Values obtained for: the mass flow [kg/s], P_{c1} and P_{c2} pressures [Pa], by changing the C_{v1} coef., (C_{b1} **=0.1355**, default value). Columns in **bold**: Results obtained for the default value of C_{b1}.

P_1 [$\times 10^5$ Pa]	C_{v1}=4.0			C_{v1}=**7.1**			C_{v1}=10.0		
	$\dot{m}$	P_{c1}	P_{c2}	$\dot{m}$	P_{c1}	P_{c2}	$\dot{m}$	P_{c1}	P_{c2}
1.50	0.38	53,573	59,552	**0.38**	**53,068**	**58,894**	0.38	51,675	57,051
1.64	0.43	42,822	50,263	**0.42**	**42,030**	**49,292**	0.43	41.025	47,808
1.85	0.48	26,544	36,229	**0.49**	**25,773**	**35,288**	0.49	24,917	34,093
2.02	0.53	13,384	24,867	**0.53**	**12,629**	**23,916**	0.53	11,646	22,692
2.10	0.54	6,783	19,056	**0.55**	**6,189**	**18,194**	0.55	5,452	17,079
2.20	0.57	3,547	15,314	**0.57**	**3,545**	**14,933**	0.57	3,540	9,322
2.30	0.59	3,540	10,939	**0.59**	**3,545**	**9,855**	0.59	3,540	3,540
2.40	0.61	3,540	3,541	**0.61**	**3,540**	**3,544**	0,61	3,540	3,540
2.50	0.62	3,540	3,540	**0.62**	**3,540**	**3,540**	0,62	3,540	3,540

Surprisingly, the results obtained show that changes in coefficient β^*_∞, a 'local coefficient', allow to obtain a better fitting in the pressure than with $\beta_{1,inner}$, being the last a 'global coefficient'.

Comparisons between the CFD results obtained in the present work and Coussirat et al., 2016 show that it is possible to obtain results of similar quality to the ones obtained using bigger meshes. This improvement is reached by means of a suitable calibration of the aforementioned coefficients, both for the SA and the SST k-ω models.

Finally, comparisons of the vapor fraction and ν_t fields computed changing the coefficients values were carried out, and they are shown in Fig.8 and Fig.9 for some values of the analysed parameters (C_{v1} and β_∞^* for the SA and SST k-ω models respectively).

Table 5: CFD results for SST k-ω/Singhal combination of models, 12,800 cells mesh and variable values of P_1. Values obtained for: the mass flow [kg/s], P_{c1} and P_{c2} pressures [Pa], by changing values of the $\beta_{1,inner}$, a 'global parameter', closely related to α^*, affecting directly ν_t , Eq.4 (see Ansys, 2015 for details). Columns in **bold**: Results obtained for the reference (default) value of $\beta_{1,inner}$**=0.075 and** β^*_∞**=cte=0.09**

P_1 [$\times 10^5$ Pa]	$\beta_{1,inner}$=0.015			$\beta_{1,inner}$=0.025			$\beta_{1,inner}$**=0.075**		
	$\dot{m}$	P_{c1}	P_{c2}	$\dot{m}$	P_{c1}	P_{c2}	$\dot{m}$	P_{c1}	P_{c2}
1.64	0.42	59,108	80,619	0.42	50,596	64,198	**0.42**	**47,072**	**57,448**
1.85	0.48	47,946	74,797	0.48	36,728	54,558	**0.48**	**32,123**	**45,666**
2.02	0.53	35,514	64,187	0.53	25,420	46,465	**0.52**	**20,043**	**35,676**
P_1 [$\times 10^5$ Pa]	$\beta_{1,inner}$=0.095			$\beta_{1,inner}$=0.125			$\beta_{1,inner}$=0.525		
	$\dot{m}$	P_{c1}	P_{c2}	$\dot{m}$	P_{c1}	P_{c2}	$\dot{m}$	P_{c1}	P_{c2}
1.64	0.42	45,660	55,719	0.43	45,684	55,472	0.42	46,700	55,076
1.85	0.48	30,144	43,271	0.48	30,586	43,329	0,48	31,491	42,438
2.02	0.53	17,572	33,180	0.53	17,578	32,763	0.53	19,146	32,168

Table 6: CFD results from SST k-ω/Singhal combination of models, 12,800 cells mesh and variable values of P_1.Values obtained for: the mass flow [kg/s], P_{c1} and P_{c2} pressures [Pa], by changing the β_∞^*, coeff., (related to the dissipation of turbulent kinetic energy, k, Eq.5). Columns in **bold**: Results obtained for the reference (default) value β^*_∞=**0.09** and $\beta_{1,inner}$=**cte=0.075.** The symbol * points that there is some convergence problems (normalised, mass residuals only reach 10^{-2}-10^{-3} orders)

P_1 [$\times 10^5$ Pa]	β^*_∞=0.20			β^*_∞=0.18			β^*_∞=0.15		
	$\dot{m}$	P_{c1}	P_{c2}	$\dot{m}$	P_{c1}	P_{c2}	$\dot{m}$	P_{c1}	P_{c2}
1.64	0.53	3,540	3,540	0.44	33,704	32,717	0.44	34,510	35,494
1.85	0.49*	3,540	3,540	0.50*	3,540	3,540	0.50	16,879	19,386
2.02	0.53*	3,540	3,540	0.50*	3,540	3,540	0.54	8,688	10,079
P_1 [$\times 10^5$ Pa	β^*_∞**=0.09**			β^*_∞=0.07			β^*_∞=0.05		
	$\dot{m}$	P_{c1}	P_{c2}	$\dot{m}$	P_{c1}	P_{c2}	$\dot{m}$	P_{c1}	P_{c2}
1.64	**0.42**	**47,072**	**57,448**	0.42	46,934	57,811	0.42	46,837	52,219
1.85	**0.48**	**32,123**	**45,666**	0.48	31,794	46,025	0.48	31,176	38,776
2.02	**0.52**	**20,043**	**35,676**	0.53	19,550	36,495	0.52	18,778	27,742

Vapor fraction and ν_t fields from Fig.8 show their low sensitivity to changes in the C_{v1} coefficient. Although there is a better prediction of the P_{c1} and P_{c2} values, Table 4 shows that they do not still reach the vapor pressure values as experiments show. On the other hand, vapor fraction and ν_t fields from Fig. 9 show a high sensitivity of them to changes in β_∞^* coefficient.

Notice that a lower value of ν_t is predicted by using both, lower or higher values of β_∞*, compared to the reference one, but the vapour fraction prediction is improved by using higher values of β_∞*, see also Table 6. It is remarked again that the influence of the $\beta_{1,inner}$ coefficient over the prediction of P_{c1} and P_{c2} is low, see Table 5, despite some improvement in the trend were reached (e.g., $\beta_{1,inner}$=0.125). Again, notice that the variation is non- monotonic because both higher and lower $\beta_{1,inner}$ values improve the predictions.

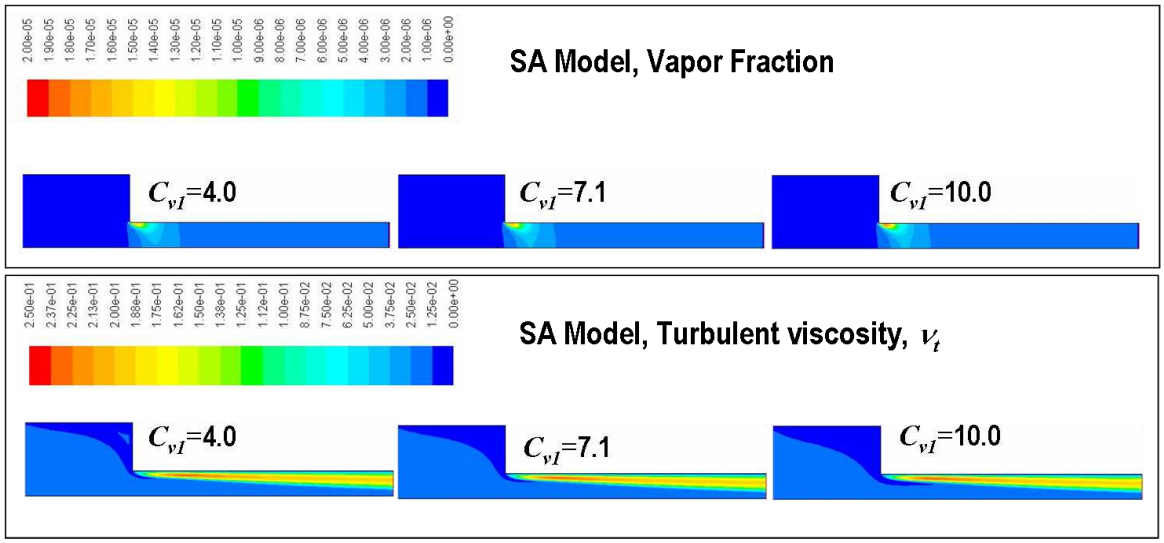

Fig. 8: Vapor fraction and ν_t fields obtained by CFD (SA/Singhal models). Results presented are from the sensitivity analysis: P_1=2.02×105Pa, and changes in the C_{v1} coeff., (C_{b1}=cte=0.1255, see Table 4).

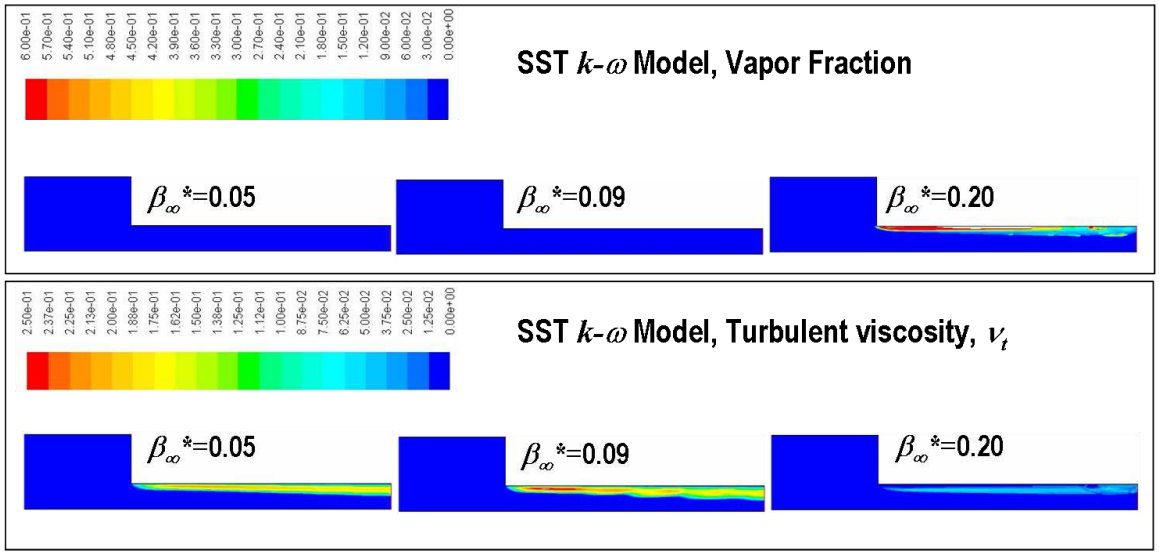

Fig. 9: Vapor fraction and ν_t fields obtained by CFD (SST k-ω/Singhal models). Results presented are from the sensitivity analysis: P_1=2.02×105Pa, and changes in the β_∞* coeff., ($\beta_{1,inner}$=cte=0.075, see Table 6).

4 CONCLUSIONS

A CFD simulation for cavitating flow in nozzles has been carried out by using combinations of two turbulence models (SA and SST k-ω) and one for cavitation (Singhal).

By using the default values for some of the available calibration coefficients in the turbulence models, a good adjustment for the coefficient C_d was obtained. Instead, the pressure variations adjustments were of less quality. This fact proves the idea already suggested in Coussirat et al., 2016 related to the poor quality of CFD results obtained by several authors that perform validation/calibration tasks for cavitation models in nozzles only taking into account the fitting for the coefficient C_d, without accounting for the local variables variation (e.g., wall pressures, local velocity profiles, and local vapor fraction profiles).

Following the ideas from Bardow et al., 2008, Coutier-Delgosha et al., 2003 and Spalart and Allmaras et al., 1994, a sensitivity analysis of the fitting parameters provided by the developers of the aforementioned turbulence models was carried out. It is remarked that the parameters selected for this sensitivity study are closely related to the turbulence viscosity, ν_t, or its production or its dissipation).

It was demonstrated that pressure adjustments can be improved by means of a suitable calibration of these parameters, showing that it will be possible to improve the cavitation inception prediction using coarser meshes than the ones used without any calibration of these coefficients. Afterwards, a suitable calibration of the turbulence model used could save computational resources because coarser meshes could be defined.

Also, this technique could be useful for unsteady simulations of cavitating flows because lower levels of ν_t provoke the apparition of unsteady flow structures. In general, the EVMs models applied in regions of refined meshing, i.e., boundary layer meshes or adaptive meshing techniques, where unsteadiness appears, the turbulence kinetic energy production increases, which results in an increased level of ν_t. High levels of ν_t dampen out the unsteady flow structures. Lowering the level of ν_t in these zones could improve the simulations of unsteadiness in the flow.

Experiments from Nurick showed that flipping flow is present almost at the same time that the cavitation inception for a L/d ratio range between $5 \leq L/d \leq 10$. This fact, points out that the cavitation inception induces the flipping phenomenon. Therefore, a good prediction of the cavitation inception will be related to the numerical prediction of the initial instability that leads to the flipping flow. Then, when the computed values for wall pressures by CFD are nearer to the measured ones under cavitating flow conditions, a better observation of the initial instabilities that induce the flipping onset, as can be seen in Fig.8 and Fig.9. The SST k-ω model with a careful calibration, predicts lower turbulent viscosity values allowing better pressure predictions and the possibility to observe the initial instabilities related to the flipping flow onset.

ACKNOWLDEDGEMENTS

Current work was partially supported by the Universidad Tecnológica Nacional (UTN) within its own research programme (UTN/SCTyP). Authors would like to express their appreciation to the UTN for providing financial support for this study (research projects UTI3504TC, and UTI3543TC).

REFERENCES

ANSYS Inc., ANSYS/FLUENT Software,
http://www.ansys.com/Industries/ Academic/Tools/, 2015.
Bardow A., Bischof C. and Bucker H. Sensitivity-Based Analysis of the k-ε Model for the Turbulent Flow Between Two Plates. *Chemical Engineering Science*, 63:4763 – 4775, 2008.
Barre S., Rolland J., Boitel G., Goncalves E. and Fortes Patella R. Experiments and Modeling of Cavitating Flows in Venturis: attached sheet cavitation. *European Journal of Mechanics B/Fluids* 28, pp. 444-464, Elsevier, 2009.
Brennen C. *Cavitation and Bubble Dynamics*. Oxford University Press, 1995.
Brennen C. A Review of Cavitation Uses and Problems in Medicine. *Cavitation: Turbo-machinery & Medical Applications Warwick University, WIMRC FORUM*, UK, 2006.
Brennen C. Cavitation in Medicine. *Interface focus: a theme supplement of Journal of the Royal Society interface* Oct 6;5(5):20150022. doi: 10.1098/rsfs.2015.0022, 2015.
Cappa F., Moll F., Coussirat M., Gandolfo E., Fontanals A. and Guardo A. Estudio de sensibilidad de parámetros de modelos en flujos cavitantes en régimen no estacionario. *Proceedings ENIEF 2014* (in Spanish).
Chunekar A. Numerical Modeling and Simulation of Turbulence–Cavitation Interactions in a Venturi Geometry. *M.Sc. Thesis, Purdue University*, West Lafayette, IN, USA, 2009.
Coussirat M. Theoretical/Numerical Study of Flows with Strong Streamlines Curvature. *PhD Thesis, Universitat Politècnica de Catalunya*, Spain, 2003.
Coussirat M., Moll F., Cappa F, and Fontanals A. Study of Available Turbulence and Cavitation Models to Reproduce Flow Patterns in Confined Flows. *ASME Journal of Fluids Engineering* 2016 (In press).
Coutier-Delgosha O., Fortes-Patella R., and Reboud J. Evaluation of the Turbulence Model Influence on the Numerical Simulation of Unsteady Cavitation. *ASME J. Fluids Eng*., 42, pp. 527–548, 2003.
Durbin P. and Pettersson R. *Statistical Theory and Modeling for Turbulent Flows*. 1^{era}edition, Wiley 2001.
Franc J. and Michel J., *Fundamentals of Cavitation.* Kluwer Academic Publishers, 2004.
Gandolfo E., Cappa F., Moll F., Coussirat M., Fontanals F. and Guardo A. Validacion/calibracion de modelos para flujos cavitantes, aplicación al diseño en ingeniería. *Proceedings ENIEF'2013* (in Spanish), 2013.
Goncalves E., Fortes-Patella R. Numerical Simulations of Cavitating Flows with Homogeneous Models. *Computer & Fluids*, pp 1682-1696, Elsevier, 2009.
Gopalan S., and Katz J. Flow Structure and Modeling Issues in the Closure Region of Attached Cavitation. *Phys. Fluids,* **12**(4), pp. 895-911, 2000.
Knapp R., Daily J. and Hammit F. *Cavitation.* McGraw-Hill, New York, 1970.
Kubota A., Kato H. and Yamaguchi, H. A New Modeling of Cavitating Flows: A Numerical Study of Unsteady Cavitation on a Hydrofoil Section. *J. Fluid Mech.*, 240, pp. 59–96, 1992.
Kunz R., Boger D., Chyczewski T., Stinebring D., Gibeling H. and Govindan, T. Multi-Phase CFD Analysis of Natural and Ventilated Cavitation About Submerged Bodies. *3rd ASME/JSME Joint Fluids Engineering Conference*, San Francisco, CA, pp. 18–23, 1999.
Li H. Kelecy F. Egelja-Maruszewski A. and Vasquez S. Advanced Computational Modeling of Steady And Unsteady Cavitating Flows. *Proceedings of IMECE2008, ASME International Mechanical Engineering Congress and Exposition*, Boston, Massachusetts, USA, 2008.
Lu Y., Wang X. and Kang Y. Simulation of Cavitation Jet Flow in a Convergent-Divergent Nozzle Water Jet. *Journal of China University of Petroleum* 33(6), pp 57–60, 2009.
Menter F. Two Equations Eddy-Viscosity Turbulence Models for Engineering Applications.

AIAA Journal, 32(8), pp. 1598–1605, 1994.
Menter F., Kuntz M., and Langtry R. Ten Years of IndustrialExperience With the SST Turbulence Model. *Turbulence, Heat and Mass Transfer*, Vol.4, K. Hanjalic, et al., eds., House, pp. 625–63, 2003.
Menter F., and Egorov Y. The Scale-Adaptive Simulation Method for Unsteady Turbulent Flow Predictions—Part 1: Theory and Model Description. *Flow Turbul. Combust.*, 85(1), pp. 113–138, 2010.
Moll F., Manuele D., Coussirat M., Guardo A. and Fontanals A. Caracterización del tipo de cavitación mediante dinámica computacional de fluidos para posteriores aplicaciones al estudio experimental del daño de cavitación. *Proceedings ENIEF 2011*, (in Spanish), 2011.
Moll F., Manuele D., Coussirat M., Cappa F., Gandolfo E., Guardo A. and Fontanals A. Optimización de un banco de ensayos de cavitación mediante fluidodinámica computacional orientado al estudio experimental del daño por cavitación. *Proceedings MECOM 2012*, (in Spanish), 2012.
Nurick W., Orifice Cavitation and its Effect on Spray Mixing. *ASME J. Fluids Eng.*, 98(2), pp 681-687, 1976.
Peterson F., Discussion: Orifice Cavitation and Its Effect on Spray Mixing. *ASME J. Fluids Eng.*, 99(2), pp. 426–427 (Nurick, W. H., 1976, J. Fluids Eng. 98(2), 681–687), 1977.
Rodio M. and Abgrall R. An Innovative Phase Transition Modeling for Reproducing Cavitation Through a Five-Equation Model and Theoretical Generalization to Six and Seven-Equation Models. *Int. J. Heat Mass Transfer*, 89, pp. 1386–1401, 2015.
Sagaut P., *Large Eddy Simulation for Incompressible Flows: An Introduction*. Springer, Berlin, 2006.
Salvador F., Martínez-López J., Romero J., and Roselló M. Computational Study of the Cavitation Phenomenon and Its Interaction with the Turbulence Developed in Diesel Injector Nozzles by Large Eddy Simulation (LES). *Math. Comput. Model.*, 57, pp. 1656–1662, 2013.
Senocak I, *Computational Methodology for the Simulation of Turbulent Cavitating Flows,*, Ph.D. Thesis, University of Florida, USA, 2002.
Senocak I. and Shyy W. Evaluation of Cavitation Models for Navier Stokes Computations. *Proceedings of FEDSM02*, *ASME Fluids Division Summer Meeting*, Montreal, Quebec, Canada. 2002.
Singhal A., Athavale M., Li H. and Jiang Y. Mathematical Basis and Validation of Full Cavitation Model, *ASME J. Fluids Eng.*, 124(3), pp. 617–624, 2002.
Sou A., Biçer B. and Tomiyama A. Numerical Simulation of Incipient Cavitation Flow in a Nozzle of Fuel Injector. *Comput. Fluid*, 103, pp. 42–48, 2014.
Spalart P. and Allmaras R. A One-Equation Turbulence Model for Aerodynamic Flows. *Rech. Aeroespatiale*, 1, pp. 5–21, 1994.
Spalart P., Strategies for Turbulence Modelling and Simulations. *Int. J. Heat Fluid Flow* 21, pp. 252–263, 2000.
Stutz B. and Reboud J. Two Phase Flow Structure of Sheet Cavitation. *Phys. Fluids* 9(12),. American Institute of Physics, pp. 3678-3686, 1997a.
Stutz B. and Reboud J. Experiment on Unsteady Cavitation. *Experiments in Fluids* 22, pp. 191-198, Springer-Verlag, 1997b.
Stutz B. and Reboud J. Measurements Within Unsteady Cavitation. *Experiments in Fluids* 39, pp. 545-552, Springer-Verlag, 2000.
Tennekes H. and Lumley L., *A First Course in Turbulence,*, MIT Press, 1972.
Vaidyanathan R., Senocak I., Wu J. and Shyy W. Sensitivity Evaluation of a Transport-Based Turbulent Cavitation Model. *ASME J. Fluids Eng.*, 125, pp 447-458, 2003.
Versteeg H. and Malalasekera W. *An Introduction to Computational Fluid Dynamics: The*

Finite Volume Method. Addison-Wesley, 1996.
Wilcox D, *Turbulence Modeling for CFD.* La Cañada Inc, DCW Industries 1994.
Zwart P., Gerber A. and Thabet B. A Two-Phase Flow Model for Predicting Cavitation Dynamics. *International Conference Multiphase Flow (ICMF)*, Yokahama, 2004.
Zhang H. Han B. Yua X. and Ju D. Numerical and Experimental Studies of Cavitation Behavior in Water-jet Cavitation Peening., *Processing Shock and Vibration* 20, pp 895–905, 2013.